Lawrence Berkeley National Laboratory

Title
Controlled Chemical Doping of Semiconductor Nanocrystals Using Redox Buffers

Permalink
https://escholarship.org/uc/item/0fh1920w

Author
Engel, Jesse H.

Publication Date
2012-05-31

DOI
10.1021/ja305293e

Peer reviewed

Controlled Chemical Doping of Semiconductor Nanocrystals Using Redox Buffers

Jesse H. Engel,[†,‡,⊥] Yogesh Surendranath,[†,§,⊥] and A. Paul Alivisatos*[,†,‡]

[†]Department of Chemistry, University of California, Berkeley, California 94720, USA,

[‡]Materials Sciences Division, Lawrence Berkeley National Laboratory, Berkeley, California 947203, USA,

[§]Miller Institute for Basic Research in Science, University of California, Berkeley, California 94720, USA.

ABSTRACT: Semiconductor nanocrystal solids are attractive materials for active layers in next generation optoelectronic devices; however, their efficient implementation has been impeded by the lack of precise control over dopant concentrations. Herein, we demonstrate a chemical strategy for the controlled doping of nanocrystal solids under equilibrium conditions. Exposing lead selenide nanocrystal thin films to solutions containing varying proportions of decamethylferrocene and decamethylferrocenium, incrementally and reversibly increases the carrier concentration in the solid by two orders of magnitude from their native values. This application of redox buffers for controlled doping establishes a new paradigm for the precise control of majority carrier concentration in porous semiconductor thin films.

Figure 1. Equilibrium oxidation of a PbSe nanocrystal solid by Fc^{*+} accompanied by PF_6^- counterion infiltration into the film.

Semiconductor nanocrystal solids are a novel class of solution-processable, modular materials that have seen increasing use as active layers for next generation optoelectronic devices.[1-3] These solids consist of macroscopic arrays of colloidally synthesized nanoparticles, wherein the band gap and the electronic properties of the composite array can be tuned by varying the size[4] and surface chemistry[5] of the constitutive elements, respectively. However, colloidally synthesized nanocrystals typically exhibit low impurity concentrations,[6] requiring post-synthetic treatments to effectively dope the nanocrystal solid.

Chemical doping methods reported[6-9] to date have primarily relied on exergonic reactions in which stoichiometric or kinetic limitations are used to control the degree of doping instead of direct modulation of the Fermi level under equilibrium conditions. For these approaches, the final doping density and homogeneity within the nanocrystal film is a complex convolution of unknown reaction rates for charge transfer, surface coordination, and/or diffusion. Indeed, the precise mechanism of doping remains ill-defined in most cases,[10,11] making a kinetic description intractable at present. In contrast to chemical methods, thermodynamic control of doping has been achieved using electrochemical methods, which shift the Fermi level of the nanocrystal solid through reversible charge transfer from the electrode.[12-16] Fine control over the applied potential (± 1 mV) allows the doping level to be set with precision. Despite this advantage, electrochemical doping methods are not suited to large area solution processing of nanocrystal solids and require specialized equipment.
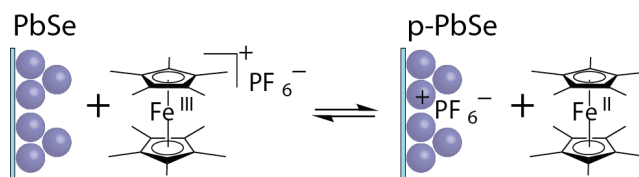
We, herein, combine the precision afforded by electrochemical doping methods with the simplicity and scalability of chemical methods by using redox buffers to fine tune the Fermi level of the film through reversible charge transfer from *solution* (Figure 1). Using a redox buffer, the solution potential can be easily tuned over a range of at least 180 mV positive and negative of the standard potential, E^0, of the reagent by varying the concentration ratio of the oxidized and reduced species (SI). Owing to the wide array of available redox reagents, displaying over a 3 V range in standard potential,[17] we envisioned that exposing nanocrystal solids to an appropriate redox buffer solution would allow for precise thermodynamic control over the dopant density in the film.

Here, we demonstrate controlled doping of ethanedithiol-treated lead selenide (PbSe) nanocrystal solids using the decamethylferrocene/decamethylferrocenium (Fc^*/Fc^{*+}) redox buffer. The carrier concentration, determined by field-effect transistor (FET) measurements, can be systematically, incrementally, and reversibly modulated by two orders of magnitude from their native values using this simple solution-based technique.

In order to select an energetically optimal redox couple for the p-type doping of PbSe nanocrystal thin films, we determined the energetics of our target nanocrystal substrate using cyclic voltammetry (CV) (Figure 2). Colloidally synthesized PbSe nanocrystals were deposited onto indium-tin-oxide (ITO) coated glass pieces by sequential dip coating and were treated with ethanedithiol (EDT) to effect ligand exchange and enhance film conductivity.[10] A low temperature, −37 °C, CV of the PbSe nanocrystal-coated ITO electrodes is shown in Figure 2a. Scanning negative from the open circuit potential, a broad quasireversible cathodic wave is observed
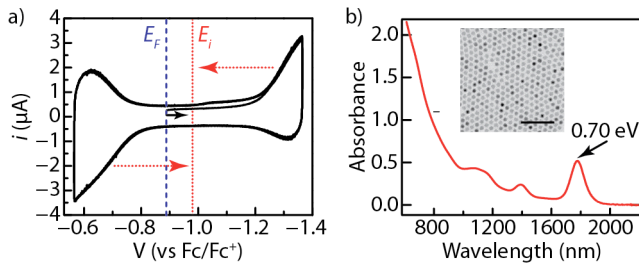
Figure 2. (a) Low temperature, −37 °C, cyclic voltammogram of an EDT-treated PbSe nanocrystal solid cast onto an ITO working electrode recorded in acetonitrile containing 0.1 M Bu_4NPF_6. Scan initiated from the open-circuit potential, E_f (— — —), in the negative direction (black arrow) at 200 mV/sec. Dotted red arrows serve as guides to the eye indicating the potential, E_i (■ ■ ■), equally separated from the rising anodic and cathodic waves as calculated in Figure S4. (b) Optical absorbance spectra of PbSe nanocrystals dispersed in carbon tetrachloride exhibiting a first exciton feature at 0.70 eV (1777 nm). Inset: Transmission electron micrograph of PbSe nanocrystals. Scale bar corresponds to 50 nm.

beginning at −1.2 V (vs Fc/Fc$^+$) and a broad quasireversible anodic wave is observed beginning at −0.8 V on the return scan. Cycling the electrode over this potential range multiple times (5 cycles are shown in Figure 2a) does not cause a significant decrease in the current response for either the cathodic or anodic waves. Additionally, scans taken with a switching potential prior to the cathodic feature also exhibit the anodic wave at −0.8 V (Figure S1). Together, these observations indicate that the anodic and cathodic waves are not dependent on each other and that the Faradaic current is representative of charge injection rather than parasitic decomposition reactions. These observations are consistent with prior low temperature CV studies,[12,13,14] and contrast with the irreversible waves observed[18,19] at room temperature. At −37 °C trapping and decomposition reactions are suppressed such that the potentials of cathodic and anodic charge injection closely approximate the thermodynamic potentials of the electron acceptor and donor states in the film, respectively. Indeed, the ~0.6 V separation of cathodic and anodic features is comparable to the energy of the first exciton feature, 1777 nm, 0.7 eV (Figure 2b), of the 6.5 ± 0.3 nm PbSe nanocrystals (Figure S2 and S3) from which the film was cast. Using the average of the potentials at which the same current for electron and hole injection into the film is observed (Figure 2a and S4) we estimate a mid-point potential, E_i, of −0.98 ± 0.01 V, corresponding to the Fermi level expected for an intrinsically doped (E_i) nanocrystal film. Importantly, this value is more negative than the open circuit potential of the native film (−0.89 V; Figure 2a, — — —) indicating that the as prepared nanocrystal solid is slightly p-type. We note that the estimation of E_i is crude given that the cathodic wave is less reversible than the anodic wave.[20] Notwithstanding, the p-type nature implied by the CV data is in line with electrical measurements of EDT-treated PbSe nanocrystal solids (vide infra).[21]

Using the electrochemical information obtained from low temperature CV, we construct the energy level diagram shown in Figure 3. The optical band gap of the colloidal PbSe nanocrystals is centered on an absolute energy scale relative to the Fc/Fc$^+$ redox couple using the E_i value determined from
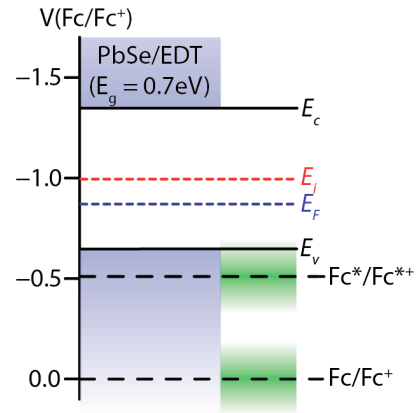

Figure 3. Energy level diagram of EDT-treated PbSe nanocrystal depicting the conduction band, E_c, valence band, E_v, Fermi level of an intrinsically doped film, E_i, native Fermi level of the as prepared PbSe film, E_f, and the standard redox potentials of the Fc*/Fc^{*+} and Fc/Fc$^+$ redox couples. Shaded green bands indicate the range of solution potentials easily accessible using Fc*:Fc^{*+} and Fc:Fc$^+$ redox buffers as given by the Nernst equation.

CV. Whereas ferrocenium (Fc$^+$) is too oxidizing to effect controlled doping of this particular PbSe film (vide infra), decamethylferrocenium's (Fc^{*+}) reduction potential is 0.51 V more negative making it an ideal candidate for p-type doping. Thus we examined the electronic effects of exposing PbSe films to Fc*/Fc^{*+} redox buffers.

Dopant density changes in the nanocrystal solid were extracted from FET measurements. Figure 4a shows that the source-drain characteristics of a freshly fabricated EDT-treated PbSe nanoparticle transistor exhibits ambipolar behavior, consistent with previous results for thiol-capped lead chalcogenide nanoparticles.[5,8] The source-drain current increases and saturates for both positive and negative values of the gate voltage, indicating injection of both electrons and holes, respectively. The ambipolar nature of the FET is also evidenced by the distinctive takeoff of current in the negative sweep direction as a result of carrier recombination.[22]

Figure 4b shows the source-drain characteristics for the same transistor after soaking in a 5 mM solution of 1:10 Fc^{*+}:Fc* in acetonitrile and then washing in pure acetonitrile. The device now functions as a unipolar transistor, depleting holes and reducing conductivity for positive gate voltages as opposed to accumulating electrons and increasing conductivity. The suppression of electron injection is also apparent in the disappearance of the takeoff feature in the negative sweeps. This change in gating behavior can be attributed to a shift in the Fermi level of the channel, as a more positive gate voltage is now required to remove the introduced holes before electrons can be injected.[23]

This shift due to doping is clearly displayed in the transfer plots shown in Figure 4c. Upon doping, electron injection is suppressed ($V_{GS} > 0$) and the transistors shift from exhibiting ambipolar to unipolar injection. Mobilities for electrons and holes in untreated films are 0.07 and 0.01 cm^2 V^{-1} s^{-1} respectively. Upon doping, only the hole mobility is measureable, and decreases slightly to 0.007 cm^2 V^{-1} s^{-1}.
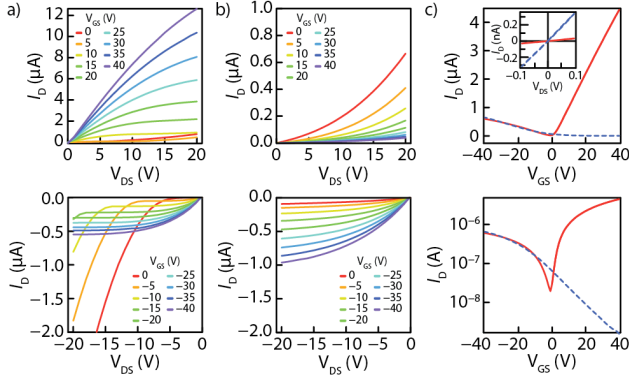
Figure 4. Drain current, I_D, as a function of drain-source voltage, V_{DS}, at a variety of gate-source voltages, V_{GS}, for a native PbSe nanocrystal film (**a**) and a PbSe nanocrystal film exposed to a 5 mM solution of 1:10 Fc^{*+}:Fc^* in acetonitrile (**b**). (**c**) I_D as a function of V_{GS} at V_{DS} = 5 V of a native (—) PbSe nanocrystal film and following doping in a 5 mM solution of 1:10 Fc^{*+}:Fc^* in acetonitrile (— — —). Data are shown on a linear (top) and logarithmic (bottom) current axis. Inset: Low field conductivity, I_D vs V_{DS}, of doped (— — —) and native (—) PbSe nanocrystal films held at V_{GS} = 0 V.

Figure 5. Small field conductivity, σ (— — —), linear field-effect mobility, μ (■ ■ ■), and hole majority carrier density, n_h (—), of PbSe nanocrystal solid films as a function of the potential of the Fc^*/Fc^{*+} doping solution. The potential of the native film (first point on left) is taken as the room temperature open circuit potential measured in acetonitrile containing 0.1 M Bu_4NPF_6 and is the average of five measurements of independently prepared films cast onto ITO coated electrode. Error bars in the electronic properties represent the geometric standard deviations about the geometric mean of at least nine devices on three independently prepared and doped nanocrystal films.

While the mobility decreases with doping, the small-field conductivity (σ) of the film (Figure 4c inset) rises from 1.4×10^{-6} to 1.5×10^{-5} S cm^{-1}. Following the Ohmic definition of the channel conductivity,[24] $\sigma = n_h e \mu$, where n_h is the density of hole majority carriers (cm^{-3}), e is the charge of an electron, and μ is the linear field-effect mobility, the carrier concentration of the film rises from 5×10^{14} cm^{-3} to 1.4×10^{16} cm^{-3} upon doping, due to both a decrease in the mobility and increase in the conductance. Notably, none of these changes are observed for films soaked only in pure acetonitrile, electrolyte (Bu_4NPF_6) in acetonitrile, or acetonitrile solutions containing only decamethylferrocene.

We investigated the dependence of doping on the redox potential of the solution by varying the Fc^{*+}:Fc^* ratio of the redox buffer. Figure 5 shows the effect on FET performance of varying the [Ox]:[Red] ratio over 3 orders of magnitude, covering a redox potential range ~180 mV to ~360 mV positive of the open circuit potential of the untreated films. Over this range, the conductivity exhibits a steady monotonic increase of ~20 times, while the linear field-effect mobility decreases by a similar magnitude, leading to carrier concentrations extracted from Ohm's law displaying an increase of two orders of magnitude. The precise origin of the decrease in field effect mobility is unclear at present, but may be due to increasing energetic site disorder[5] or partial screening of the gate field due to counterion mobility within the film.[25] X-ray photoelectron spectroscopy (XPS) failed to detect PF_6^- in the treated film (Figure S5), in line with the low observed doping levels: less than one free carrier per 100 nanoparticles for the highest doping level in Figure 5 (see SI for detailed calculation). Notwithstanding, the electronic data indicates that increasing the redox potential of the buffer solution incrementally modulates the dopant density in the film.

Importantly, the increases in carrier concentration do not correspond precisely to that expected based on the change in
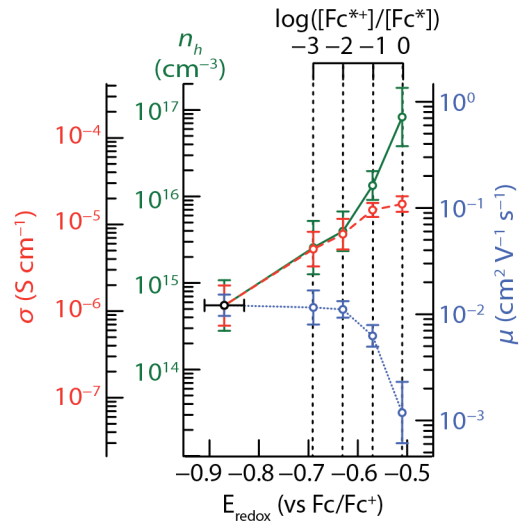
the solution potential: a ~360 mV shift in solution potential results in only ~120 meV shift the Fermi level of the film (two orders of magnitude increase in carrier concentration). In analogy to what has been documented for semiconductor/solution[26,27] junctions, we suspect that the high population of localized surface states in the nanocrystal film[20] serves to partially pin the Fermi level of the nanocrystal solid, thereby preventing a straightforward correspondence between the solution potential and carrier concentration in the film. Thus, we expect that films possessing lower surface state densities will be amenable to more efficient and stable doping using redox buffers.

To ensure that doping is occurring under thermodynamic control, we examined the time course and reversibility of the charge transfer reaction. Figure 6 illustrates changes in the dopant density, n_h, of a PbSe nanocrystal FET as a function of soaking time in a series of different Fc^*/Fc^{*+} redox buffers (see Figure S6 for raw σ and μ values). The first point was measured from untreated films which then became lightly doped to a steady state value upon soaking in a 1:1000 Fc^{*+}:Fc^* buffer. In the middle frame, the transistors were soaked in more oxidative buffers (1:100 and 1:10 for spheres and circles, respectively) and reached new steady state levels of doping corresponding to the increased oxidizing power of the buffer. In the last frame, the transistors were both soaked back in the original buffer (1:1000) and eventually reversed to their earlier levels of doping. While the frustrated kinetics of diffusion in a microporous network[28] lead to differing time scales for each system to reach equilibrium, the time invariance following equilibration and the reversibility of the attendant doping level establishes that doping occurs under
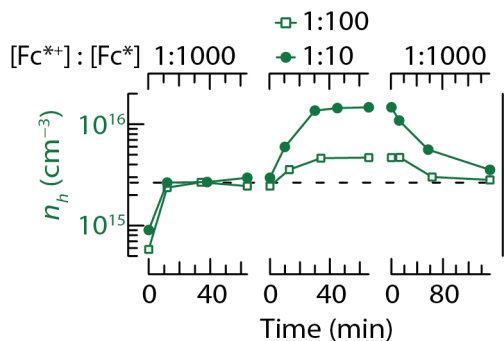
Figure 6. Hole majority carrier density, n_h (—), of two PbSe nanocrystal solid films as a function of the time duration of exposure to Fc^*/Fc^{*+} doping solutions. The initial points represent untreated films. Both films were exposed to a 5 mM 1:1000 Fc^{*+}:Fc^* doping solution in acetonitrile for the first and last time series whereas one was exposed to a 5 mM 1:10 (closed circles) and the other, a 5 mM 1:100 (open squares) Fc^{*+}:Fc^* doping solution in between.

thermodynamic control. As expected, a time invariant equilibrium doping level is not obtained when PbSe films are exposed to a solution potential well beyond the valence band edge. A monotonic increase in dopant concentration with time, indicative of kinetically limited doping, occurs when PbSe films are exposed to highly oxidixing Fc^+ solutions (Figure S7).

The equilibrium between the nanoparticle film and the redox buffer solution is metastable, as it exists under a chemically applied electrochemical potential while soaking. When the film is removed from the solution, it settles to a new metastable equilibrium in which charge has been injected and "frozen in", even though the film no longer experiences a chemically imposed potential. Figure S8 shows that the extracted carrier concentration drops over this initial period, but then levels out to a steady value. Thus, despite some initial reconfiguration, a large fraction of free carriers remains, leaving films whose doping concentrations are controllable and stable.

In conclusion, we have demonstrated that PbSe nanocrystal solids can be controllably doped p-type under thermodynamic control by exposure to Fc^*/Fc^{*+} redox buffers. Studies are underway to extend this doping strategy to n-type doping as well as to other materials systems.

ASSOCIATED CONTENT

Full experimental details, additional CVs, TEM images, sizing statistics, XPS spectra, Fc^+ doping results, and time dependence of carrier concentrations. This material is available free of charge via the Internet at http://pubs.acs.org.

AUTHOR INFORMATION

Corresponding Author

apalivisatos@lbl.gov

Author Contributions

⊥These authors contributed equally to this work.

ACKNOWLEDGMENT

REFERENCES

(1) Talapin, D. V.; Lee, J.-S.; Kovalenko, M. V.; Shevchenko, E. V. *Chem. Rev.* **2010**, *110*, 389–458.

(2) Semonin, O. E.; Luther, J. M.; Choi, S.; Chen, H.-Y.; Gao, J.; Nozik, A. J.; Beard, M. C. *Science* **2011**, *334*, 1530–1533.

(3) Tang, J.; Kemp, K. W.; Hoogland, S.; Jeong, K. S.; Liu, H.; Levina, L.; Furukawa, M.; Wang, X.; Debnath, R.; Cha, D.; Chou, K. W.; Fischer, A.; Amassian, A.; Asbury, J. B.; Sargent, E. H. *Nature Materials* **2011**, *10*, 765–771.

(4) Dai, Q.; Wang, Y.; Li, X.; Zhang, Y.; Pellegrino, D. J.; Zhao, M.; Zou, B.; Seo, J.; Wang, Y.; Yu, W. W. *Acs Nano* **2009**, *3*, 1518–1524.

(5) Liu, Y.; Gibbs, M.; Puthussery, J.; Gaik, S.; Ihly, R.; Hillhouse, H. W.; Law, M. *Nano Lett* **2010**, *10*, 1960–1969.

(6) Norris, D. J.; Efros, A. L.; Erwin, S. C. *Science* **2008**, *319*, 1776–1779.

(7) Talapin, D.; Murray, C. *Science* **2005**, *310*, 86–89.

(8) Leschkies, K. S.; Beatty, T. J.; Kang, M. S.; Norris, D. J.; Aydil, E. S. *Acs Nano* **2009**, *3*, 3638–3648.

(9) Mocatta, D.; Cohen, G.; Schattner, J.; Millo, O.; Rabani, E.; Banin, U. *Science* **2011**, *332*, 77–81.

(10) Luther, J. M.; Law, M.; Song, Q.; Perkins, C. L.; Beard, M. C.; Nozik, A. J. *Acs Nano* **2008**, *2*, 271–280.

(11) Kutana, A.; Erwin, S. C. *Phys Rev B* **2011**, *83*, 235419.

(12) Yu, D.; Wang, C.; Guyot-Sionnest, P. *Science* **2003**, *300*, 1277–1280.

(13) Liu, H.; Keuleyan, S.; Guyot-Sionnest, P. *J. Phys. Chem. C* **2012**, *116*, 1344–1349.

(14) Wehrenberg, B. L.; Yu, D.; Ma, J.; Guyot-Sionnest, P. *J. Phys. Chem. B* **2005**, *109*, 20192–20199.

(15) Houtepen, A. J.; Kockmann, D.; Vanmaekelbergh, D. *Nano Lett* **2008**, *8*, 3516–3520.

(16) Fabregat-Santiago, F.; Mora-Seró, I.; Garcia-Belmonte, G.; Bisquert, J. *J. Phys. Chem. B* **2003**, *107*, 758–768.

(17) Connelly, N. G.; Geiger, W. E. *Chem. Rev.* **1996**, *96*, 877–910.

(18) Choi, J. J.; Lim, Y.-F.; Santiago-Berrios, M. B.; Oh, M.; Hyun, B.-R.; Sun, L.; Bartnik, A. C.; Goedhart, A.; Malliaras, G. G.; Abruña, H. D.; Wise, F. W.; Hanrath, T. *Nano Lett* **2009**, *9*, 3749–3755.

(19) Jiang, X.; Schaller, R. D.; Lee, S. B.; Pietryga, J. M.; Klimov, V. I.; Zakhidov, A. A. *J Mater Res* **2007**, *22*, 2204–2210.

(20) This is in accord with the observation of significant electron trapping in PbSe films: Konstantatos, G.; Levina, L.; Fischer, A.; Sargent, E. H. *Nano Lett* **2008**, *8*, 1446–1450.

(21) Wang, R. Y.; Feser, J. P.; Lee, J.-S.; Talapin, D. V.; Segalman, R.; Majumdar, A. *Nano Lett* **2008**, *8*, 2283–2288.

(22) Zaumseil, J.; Friend, R.; Sirringhaus, H. *Nature Materials* **2006**, *5*, 69–74.

(23) Sze, S.M. & Ng, K.K. *Physics of Semiconductor Devices, Third Edition*. (John Wiley & Sons Inc.: 2007).

(24) Klem, E. J. D.; Shukla, H.; Hinds, S.; MacNeil, D. D.; Levina, L.; Sargent, E. H. *Appl Phys Lett* **2008**, *92*, 212105.

(25) Chua, L.; Zaumseil, J.; Chang, J.; Ou, E.; Ho, P.; Sirringhaus, H.; Friend, R. *Nature* **2005**, *434*, 194–199.

(26) Bard, A. J.; Bocarsly, A. B.; Fan, F. R. F.; Walton, E. G.; Wrighton, M. S. *J. Am. Chem. Soc.* **1980**, *102*, 3671–3677.

(27) Lewerenz, H. J. *J. Electroanal. Chem.* **1993**, *356*, 121–143.

(28) Havlin, S.; Benavraham, D. *Adv Phys* **1987**, *36*, 695–798.